IMAGE DEHAZING USING DARK CHANNEL PRIOR AND RELATIVITY GAUSSIAN

Developed by:

Kumar Kashyap : 20171019
Rakesh Kumar Singh : 20171044
Raushan Kumar : 20171056
Omar Farahan Molla : L20181081

Supervised by:

Prof. Biswanath Pal

Project in brief

Project title:	Image Dehazing using Dark channel prior and relativity gaussian
Organization:	University Institute of Technology
Objectives:	Image Dehazing
Supervised by:	Prof. Biswanath Pal
Technology used:	MATLAB

Abstract:

atmospheric particles affect the natural scene and the visibility will be tampered. Different dehazing methods are used to restore the visual perception of the image, increase the natural panoramic view and preserve the structural features of the image. Poor visibility becomes a significant issue for most outdoor vision applications. Image dehazing is a highlighted research area because of its real time applications in surveillance systems, driver assistance system especially for the people who resides in hilly areas where mist and haze is prominent. This paper presents a modified dark channel prior based image dehazing system with an enhanced and refined transmission map constructed by utilizing the RGB and YCrCb color system. Transmission map is constructed and estimated from combined air-light component obtained from the above said color models. In this work, we compute the Relativity of Gaussian for RGB and YCbCr color space to produce guidance image. The both guidance images thus obtained are applied to guided filter for smoothening. Finally, haze less image reconstruction is performed by utilizing the guidance images obtained from the previous step. In this proposed work, we focus on improving the transmission map by utilizing the concept of Relativity of Gaussian and Guided filter. We can find that the proposed method does not over enhance the images. Results analysis focuses on investigating the efficiency of proposed method by reconstructing the image without distortion, with no color artifacts and better aesthetic visual image.

CONTENTS

1. Introduction

Environmental impact such as haze and fog have an unfavorable effect on the image quality. It will be very difficult and challenging to use such images in driver assistance systems, monitoring surveillance systems and outdoor and indoor object detection and recognition which require clear visible and high-quality image for further processing. Usually, restoring the degraded hazy images from single input image is pretty challenging and tedious. Haze or fog is a prevalent natural phenomenon created by atmosphere particles that are suspended. Therefore, haze removal is a significant task to restore the visibility in images. There are many problems that need to be addressed in haze removal such as efficient computation of atmospheric air light and transmission depth map. Improved Dark Channel Prior (DCP) is used to improve the transmission depth map construction in our work. The contribution that we introduce focuses on a considerable betterment of the reconstruction module. DCP-based image dehazing technique is used to prevent blocking artifacts with enhanced transmission map. It calculates the three transmission maps based on each R, G, B components and one transmission map based on the luminance component of the YCrCb color system. Two images are reconstructed after applying guided filter in transmission map. In this paper, Relativity of Gaussian (RoG) and Guided filter is applied to enhance the transmission depth map for removing the existence of haze.

2. Dark channel prior based image dehazing

2.1. Degradation model:

A hazy image formed as shown in Fig. 1 can be mathematically modeled as follows:

$$I(x) = J(x)e^{-\beta d(x)} + A\left(1 - e^{-\beta d(x)}\right), \quad (1)$$

where x represents the image coordinates, I is the observed hazy image, J is the haze-free image, A is the global atmospheric light, β is the scattering coefficient of the atmosphere, and d is the scene depth. Here, e− βd is often represented as the transmission map and is given by:

$$t(x) = e^{-\beta d(x)}. \quad (2)$$

In clear weather conditions, we have β ≈ 0, and thus I ≈ J. However, β becomes non-negligible for hazy images. The first term of Eq. (1), J(x)t(x) (the direct attenuation), decreases as the scene depth increases. In contrast, the second term of Eq. (1), A(1 − t(x)) (the air light), increases as the scene depth increases. Since the goal of image dehazing is to recover J from I, once A and t are estimated from I, J can be arithmetically obtained as:

$$J(x) = \frac{I(x) - A}{t(x)} + A. \quad (3)$$

However, the estimation of A and t is non-trivial. In particular, since t varies spatially according to the scene depth, the number of unknowns is equivalent to the number of image pixels. Thus, a direct estimation of t from I is prohibitive without any prior knowledge or assumptions.

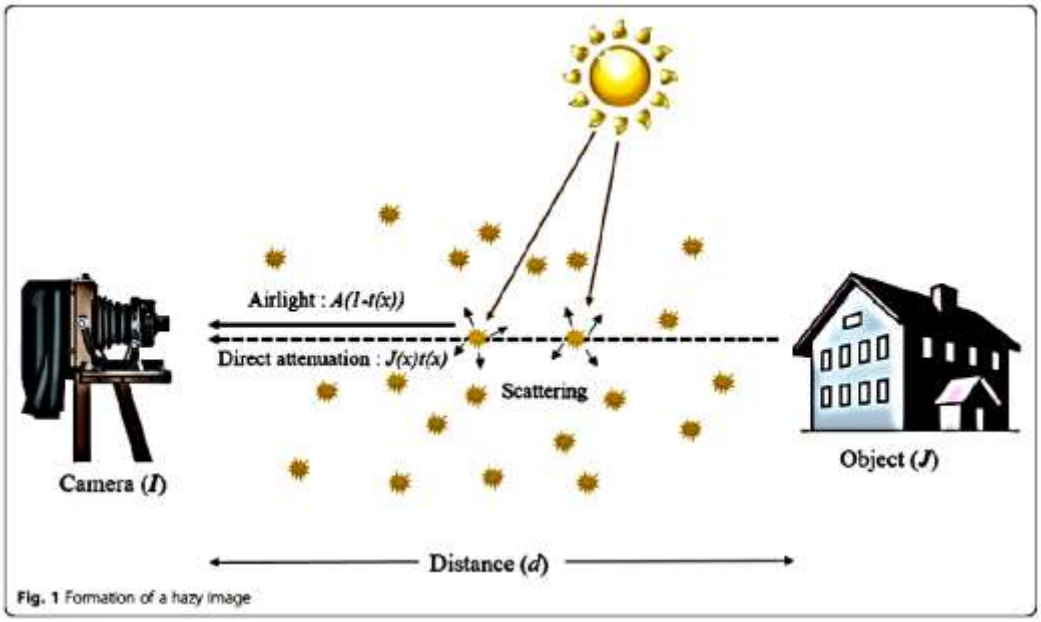

Fig. 1 Formation of a hazy image

2.2. Dark channel prior (DCP):

performed an empirical investigation of the characteristic of haze-free outdoor images. They found that there are dark pixels whose intensity values are very close to zero for at least one-color channel within an image patch. Based on this observation, a dark channel is defined as follows:

$$J^{\text{dark}}(x) = \min_{y \in \Omega(x)} \left(\min_{c \in \{r,g,b\}} J^c(y) \right), \tag{4}$$

where Jc is an intensity for a color channel c ∈ {r, g, b} of the RGB image and Ω(x) is a local patch centered at pixel x. According to Eq. (4), the minimum value among the three-color channels and all pixels in Ω(x) is chosen as the dark channel Jdark(x).

From 5000 dark channels of outdoor haze-free images, it was demonstrated that about 75 percent of the pixels in the dark channels have zero values and 90 percent of the pixels have values below 35 when the pixels in the sky region are excluded [10]. The low intensities in the dark channel are due to the following three main features: (i) shadows, e.g., shadows from cars and buildings in an urban scene or shadows from trees, leaves, and rocks in a landscape (Fig. 2a); (ii) colorful objects or surfaces, e.g., red or yellow flowers and leaves (Fig. 2b); and (iii) dark objects or surfaces, e.g., dark tree trunks and stones (Fig. 2c). Based on the above observation, the pixel value at the dark channel can be approximated as follows:

$$J_{\text{dark}} \approx 0 \tag{5}$$

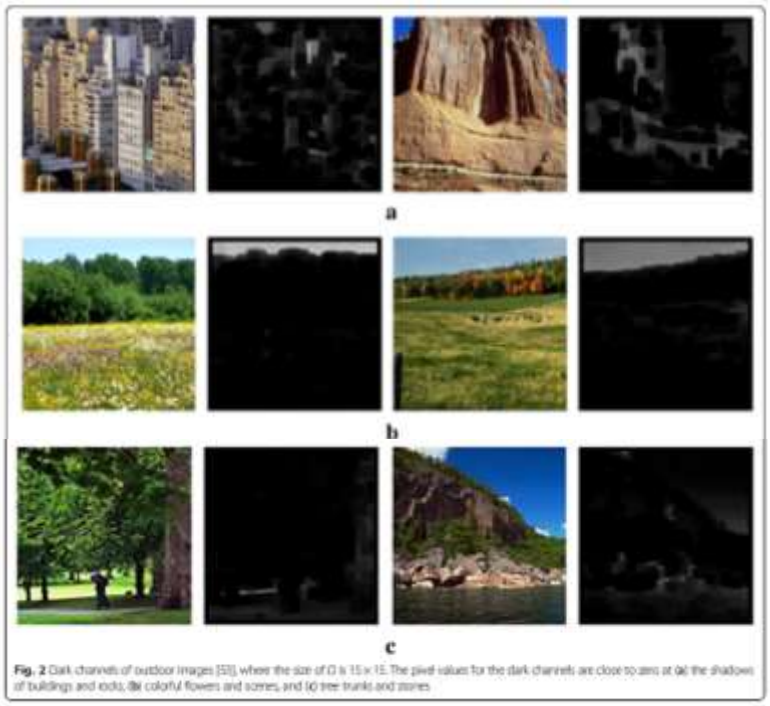

Fig. 2 Dark channels of outdoor images [53], where the size of Ω is 15 × 15. The pixel values for the dark channels are close to zero at (a) the shadows of buildings and rocks, (b) colorful flowers and scenes, and (c) tree trunks and stones

This approximation to zero for the pixel value of the dark channel is called the DCP. On the contrary, the dark channels from hazy images produce pixels that have values far above zero as shown in Fig. 3. Global atmospheric light tends to be achromatic and bright, and a mixture of air light and direct attenuation significantly increases the minimum value of the three-color channels in the local patch. This implies that the pixel values of the dark channel can serve as an important clue to estimate the haze density. Successful dehazing results of various DCP-based dehazing algorithms support the effectiveness of the DCP in image dehazing.

2.3. DCP-based image dehazing:

In the DCP-based dehazing algorithm, the dark channel is first constructed from the input image as in Eq. (4). The atmospheric light and the transmission map are then obtained from the dark channel. The transmission map is further refined, and the haze-free image is finally reconstructed as Eq. (3). More specifically, given the degradation model of

$$I(x) = J(x)t(x) + A(1-t(x)), \tag{6}$$

the minimum intensity in the local patch of each color channel is taken after dividing both sides of Eq. (6) by Ac as follows:

$$\min_{y\in\Omega(x)} \frac{I^c(y)}{A^c} = \tilde{t}(x) \min_{y\in\Omega(x)} \frac{J^c(x)}{A^c} + (1-\tilde{t}(x)). \tag{7}$$

Here the transmission in the local patch Ω(x) is assumed to be constant and is represented as ~t(x). Then, the min operator of the three-color channels can be applied to Eq. (7) as follows:

$$\min_{y\in\Omega(x)} \left(\min_{c} \frac{I^c(y)}{A^c} \right) = \tilde{t}(x) \min_{y\in\Omega(x)} \left(\min_{c} \frac{J^c(y)}{A^c} \right) + (1-\tilde{t}(x)). \tag{8}$$

According to the DCP approximation of Eq. (5), ~t(x) can be represented as

$$\tilde{t}(x) = 1- \min_{y\in\Omega(x)} \left(\min_{c} \frac{I^c(y)}{A^c} \right). \tag{9}$$

Here, the atmospheric light A needs to be estimated in order to obtain the transmission map ~t. Most of the previous single image based dehazing methods estimate A from the most haze-opaque pixels. As discussed in

Section 1.2.2, the pixel value of the dark channel is highly correlated with haze density. Therefore, the top 0.1 % of the brightest pixels in the dark channel is first selected, and the color with the highest intensity value among the selected pixels is then used as the value for A [10]. Figure 4 illustrates the process used to obtain A. If the pixel with the highest intensity value is used to estimate A, the pixels in the patches as shown in Fig. 4d, e would be selected, yielding significant estimation errors. Instead, by finding the candidate pixels from the dark channel as shown in Fig. 4b, the pixel that accurately estimates A can be found as shown in Fig. 4c. It is noted in [10] that the DCP is not reliable in the sky region. Fortunately, the color of the sky is close to A in hazy images, and thus, we have:

$$\min_{y\in\Omega(x)}\left(\min_{c}\frac{I^{c}(y)}{A^{c}}\right)\approx 1 \quad \text{and} \quad \tilde{t}(x)\approx 0. \tag{10}$$

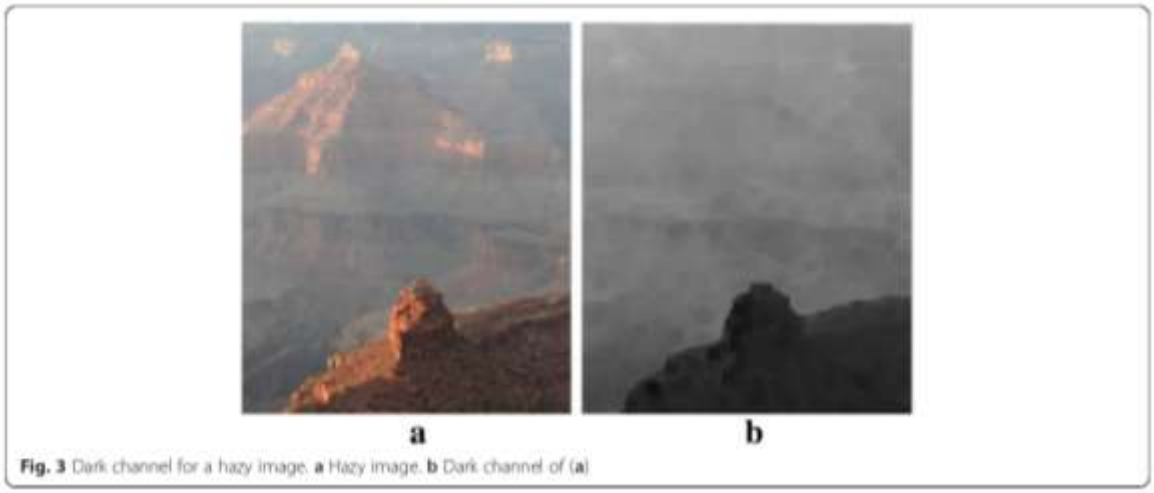

Fig. 3 Dark channel for a hazy image. **a** Hazy image. **b** Dark channel of (**a**)

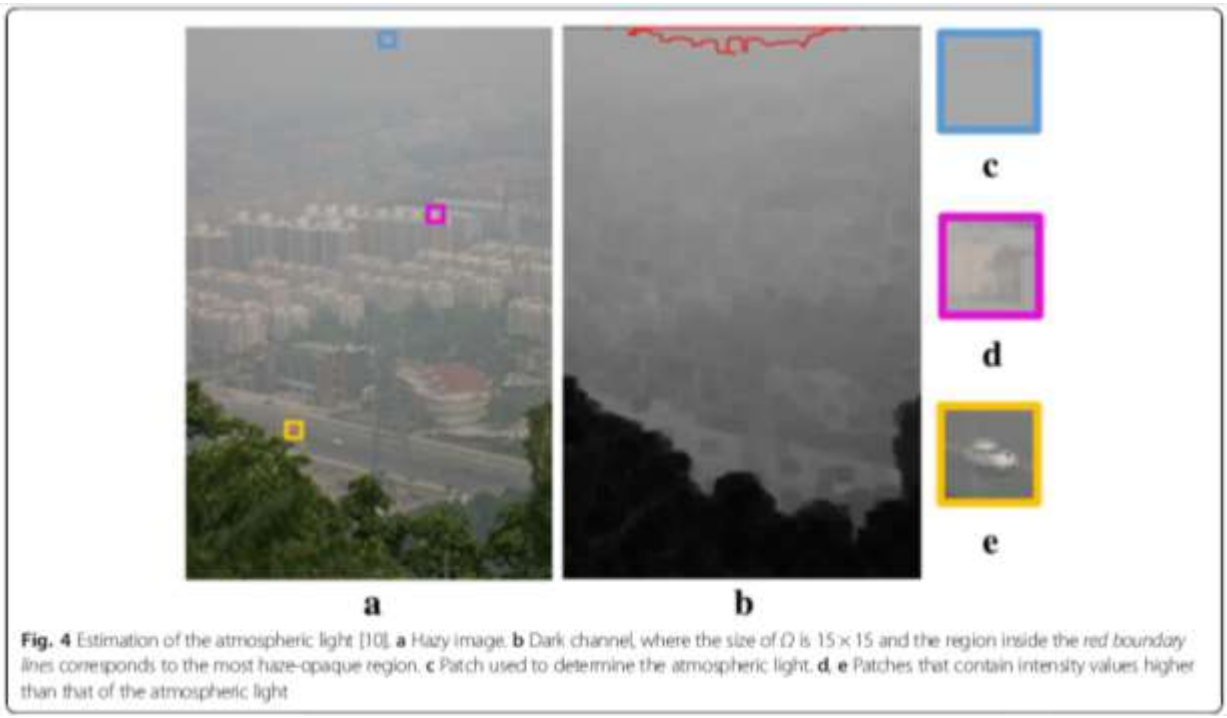

Fig. 4 Estimation of the atmospheric light [10]. **a** Hazy image. **b** Dark channel, where the size of Ω is 15 × 15 and the region inside the *red boundary lines* corresponds to the most haze-opaque region. **c** Patch used to determine the atmospheric light. **d**, **e** Patches that contain intensity values higher than that of the atmospheric light

This corresponds to the definition of t(x) because d(x) approaches infinity for the sky region. Therefore, the sky does not need special treatment for estimating the transmission map if we obtain ~t(x)as Eq. (9). Given A, ~t, and I, the dehazed image is obtained as:

$$J(x) = \frac{I(x)-A}{\max(\tilde{t}(x), t_0)} + A, \tag{11}$$

where t_0 is used as a lower bound for the transmission map.

3. Analysis of DCP-based dehazing algorithms:

In Section 2, we reviewed the original DCP-based dehazing algorithm. The follow-up methods are based on the basic structure presented in but differ in each step of the dehazing procedure. Table 1 shows the DCP-based dehazing algorithms from that are investigated in this paper. Instead of analyzing each method individually, we classify all the methods in accordance with the four steps of image dehazing and then perform a step-by-step analysis. Each of the following subsections describes and compares the various methods used for each step.

3.1. Dark channel construction:

Most conventional DCP-based dehazing methods estimate the dark channel from the input hazy image I. In Eq. (4), the size of the local patch Ω(x) is the only parameter that needs to be determined. Although the effect of the size of the local patch is significant, most conventional methods simply use a local patch with a fixed size or do not specify the size of the local patch.

Table 2 shows typical patch sizes used in the previous methods.

Figure 5a shows two hazy images. The top row in Fig. 5 corresponds to a remote aerial photograph with less local texture and heavy haze. Therefore, a small local patch is sufficient in order to estimate the dark channel, resulting in a reduction in the DCP calculation time. However, an image that has complicated local textures, as shown in the second row of Fig. 5, needs a larger local patch size to exclude false textures from the dark channel.

Note that the block-min process of Eq. (4) Inevitably decreases the apparent resolution of the dark channel as the size of the patch increases. Therefore, the minimum possible patch size that does not produce false textures in the dark channel needs to be

Table 1 Comparison of DCP-based dehazing

Step	Method		
Dark channel construction	Min filter (Eq. (4))		
	Median filter (Eq. (12))		
Atmospheric light estimation	Candidate	DCP top 0.1 %	
		DCP top 0.2 %	
		DCP maximum	
		DCP top 5 % and edge	
	Selection criterion	Intensity	
		Entropy	
Transmission map construction	Eq. (17)		
	Eq. (18)		
	(i)		
Transmission map refinement	Gaussian filter		
	Bilateral filter		
	Soft matting		
	Cross-bilateral filter		
	Guided filter		

(i) $t(x) = 1 - w\left(\log\left(\min_{c\in\{r,g,b\}} \frac{I^c(x)}{A^c}\right)\right)$

Table 2 Local patch sizes used for previous methods

Patch size
3 × 3
11 × 11
15 × 15

found for every hazy image by considering application-dependent image local details. Apart from the aforementioned general method for the dark channel estimation, Zhang replaced the minimum operator by the median operator as follows:

$$I^{\text{dark}}(x) = \underset{y \in \Omega(x)}{\text{median}} \left(\min_{c \in \{r,g,b\}} I^c(y) \right). \tag{12}$$

As a result of the median operation, the dark channels become less blurry, as shown in Fig. 6. However, the median operator is computationally more complex than the minimum operator. Moreover, the median-based method is less physically meaningful because the assumption of the DCP becomes deteriorated. As shown in the second row of Fig. 6, dense image textures remain visible for the dark channel, even when a large patch size of 15 × 15 is used. For the sake of the visibility enhancement of hazy images, however, the median filter is somewhat effective because it does not require complicated post-processing, which is necessary for smooth and blurry dark channels that are obtained by the minimum operator.

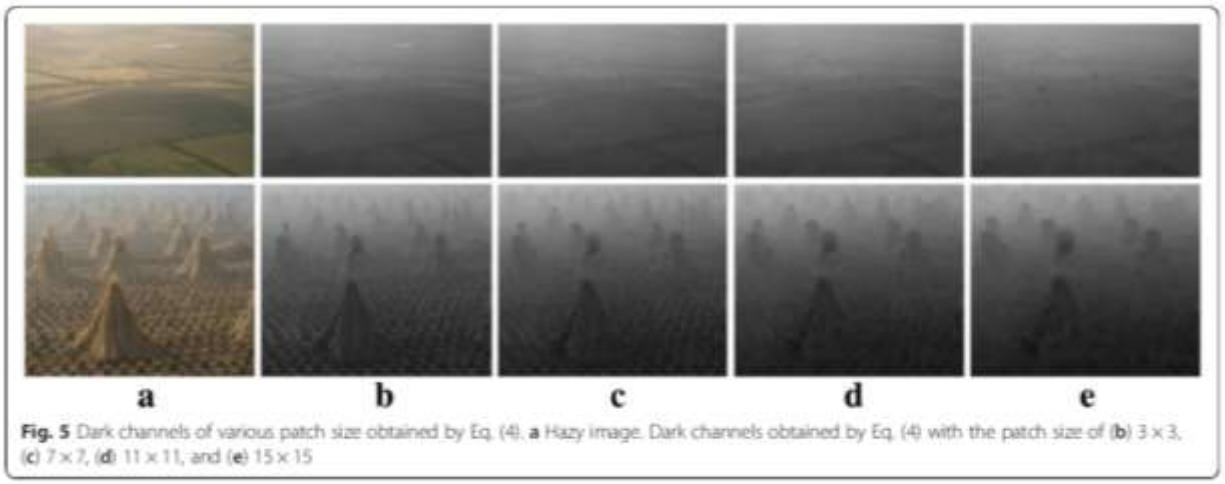

Fig. 5 Dark channels of various patch size obtained by Eq. (4). **a** Hazy image. Dark channels obtained by Eq. (4) with the patch size of (**b**) 3 × 3, (**c**) 7 × 7, (**d**) 11 × 11, and (**e**) 15 × 15

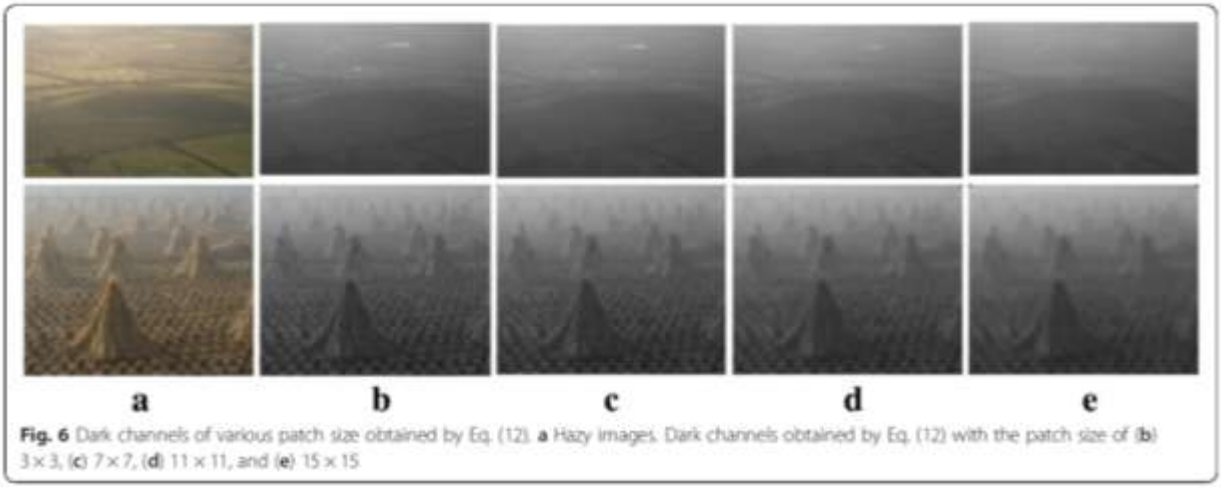

Fig. 6 Dark channels of various patch size obtained by Eq. (12). **a** Hazy images. Dark channels obtained by Eq. (12) with the patch size of (**b**) 3 × 3, (**c**) 7 × 7, (**d**) 11 × 11, and (**e**) 15 × 15

3.2. Atmospheric light estimation:

The majority of conventional DCP-based dehazing methods estimate A as described in Section 2.3. The pixel with the highest dark channel value is used directly as follows:

$$A = I\left(\text{argmax}_x\left(I^{\text{dark}}(x)\right)\right). \quad (13)$$

However, the above method can incorrectly select the pixel when the scene contains bright objects. Instead,
pixels with a top p% dark channel values are selected as the most haze-opaque pixels, and the one with the highest intensity is used to estimate A. This remains one parameter p in the estimation of A, which is empirically set as 0.1 or 0.2. To explicitly exclude bright objects from the estimation of A, the local entropy is measured as

$$E(x) = \sum_{i=0}^{N}(p_x(i) \times \log_2(p_x(i)), \quad (14)$$

where px(i) represents the probability of a pixel value I in the local patch centered at x, and N represents the
maximum pixel value. The local entropy value is low for regions with smooth variations, which highly likely correspond to haze-opaque regions. Therefore, the pixel with the lowest entropy value is used to obtain A among the highest p% pixels in the dark channel (p = 0.1). Table 3 lists the conventional methods that are used to estimate atmospheric light. To quantitatively evaluate atmospheric light estimation methods, we used the foggy road image database (FRIDA) which consists of pairs of synthetic color and depth images. For a given depth image and β, the ground-truth transmission map can be constructed as t(x) = e− βd(x). The hazy image I is then obtained as Eq. (6) by using the atmospheric light
A. Therefore, a variety of hazy images can be generated by changing β (haze density) and A (global lightness).
Figure 7 shows the average root-mean-square error (RMSE) between the ground-truth and estimated atmospheric lights for the 66 test images in the FRIDA. The RMSE is obtained as

$$RMSE = \sqrt{\frac{1}{3}\left(\left(\hat{A}_R - A_R^*\right)^2 + \left(\hat{A}_G - A_G^*\right)^2 + \left(\hat{A}_B - A_B^*\right)^2\right)}, \quad (15)$$

where $A^* = \left(A_R^* A_G^* A_B^*\right)$ and $\hat{A} = [\hat{A}_R \hat{A}_G \hat{A}_B]$ represent the ground-truth and estimated atmospheric lights, respectively. Since the candidate pixels for the

atmospheric light estimation are obtained from the dark channel, the local patch size also plays an important role in the accuracy of the estimation. When a small patch size is used, as shown in Fig. 8b, the pixels for bright objects are considered as candidate pixels, yielding inaccurate A estimates. The use of a large patch size can prevent selecting such pixels, as shown in Fig. 8c. The quantitative evaluation result as shown in Fig. 7a also supports our observation. The accuracy is rather insensitive to p when a large 32 × 32 patch is used. Therefore, a large patch size (e.g., 32 × 32) with p = 0~0.4% is effective only when the accuracy of the atmospheric light estimation is considered. One practical solution that takes into account the accuracy of both the dark channel and the atmospheric light involves using different patch sizes to estimate the dark channel estimation and atmospheric light. When the local entropy, as in Eq. (15), is used to prevent pixels of small bright objects from being selected, the estimation accuracy of the atmospheric light improves, as shown in Fig. 7b. The estimation accuracy is still best for the largest patch size of 32 × 32 and is less sensitive to the p value due to the

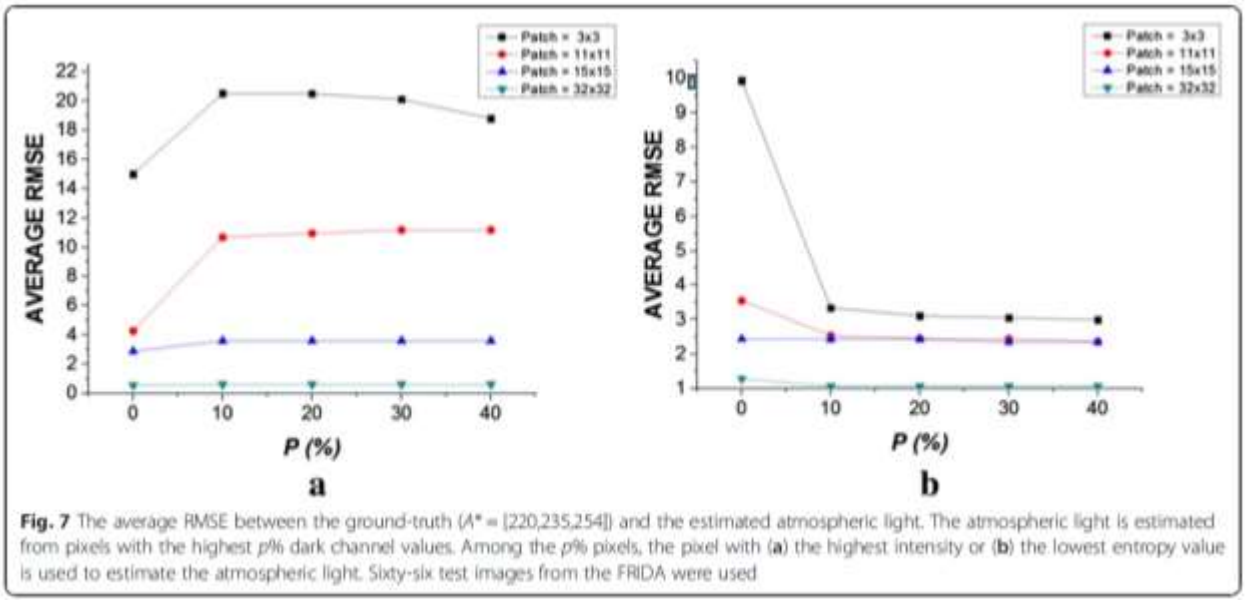

Fig. 7 The average RMSE between the ground-truth ($A^* = [220,235,254]$) and the estimated atmospheric light. The atmospheric light is estimated from pixels with the highest p% dark channel values. Among the p% pixels, the pixel with (**a**) the highest intensity or (**b**) the lowest entropy value is used to estimate the atmospheric light. Sixty-six test images from the FRIDA were used

3.3. Transmission map estimation:

The transmission map ~t(x) fined in Eq. (9) is obtained from the DCP. If the DCP

$$\tilde{t}(x) = 1 - \min_{y \in \Omega(x)} \left(\min_{c} \frac{I^c(y)}{A^c} \right) + \tilde{t}(x) \cdot \min_{y \in \Omega(x)} \left(\min_{c} \frac{I^c(y)}{A^c} \right).$$

Table 3 Conventional methods used to estimate atmospheric light

Input	Parameter	Selection criterion	Reference
Dark channel	$p = 0$	Highest intensity	[19, 20]
	$p = 0.1$	Highest intensity	
	$p = 0.2$	Highest intensity	
	$p = 0.1$	Minimum entropy	

As we observed in Section 2.2, the pixel value of the dark channel, Jdark(x), is highly likely zero, and so is (J/A)dark(x). However, if (J/A)dark(x) is not close to zero, the transmission map obtained as Eq. (9) can be under-estimated since the positive offset in Eq. (16) is always neglected [28]. In the original DCP-based dehazing method, it is mentioned that the image may look unnatural if the haze is removed thoroughly. A constant ω (0 < ω < 1) is thus used to retain a small amount of haze:

$$\tilde{t}(x) = 1 - \omega \min_{y \in \Omega(x)} \left(\min_{c} \frac{I^c(y)}{A^c} \right). \tag{17}$$

However, we consider that a better visibility in the dehazed image can be achieved with Eq. (17) because we inadvertently compensate for the under-estimation of ~t(x) by multiplying ω.

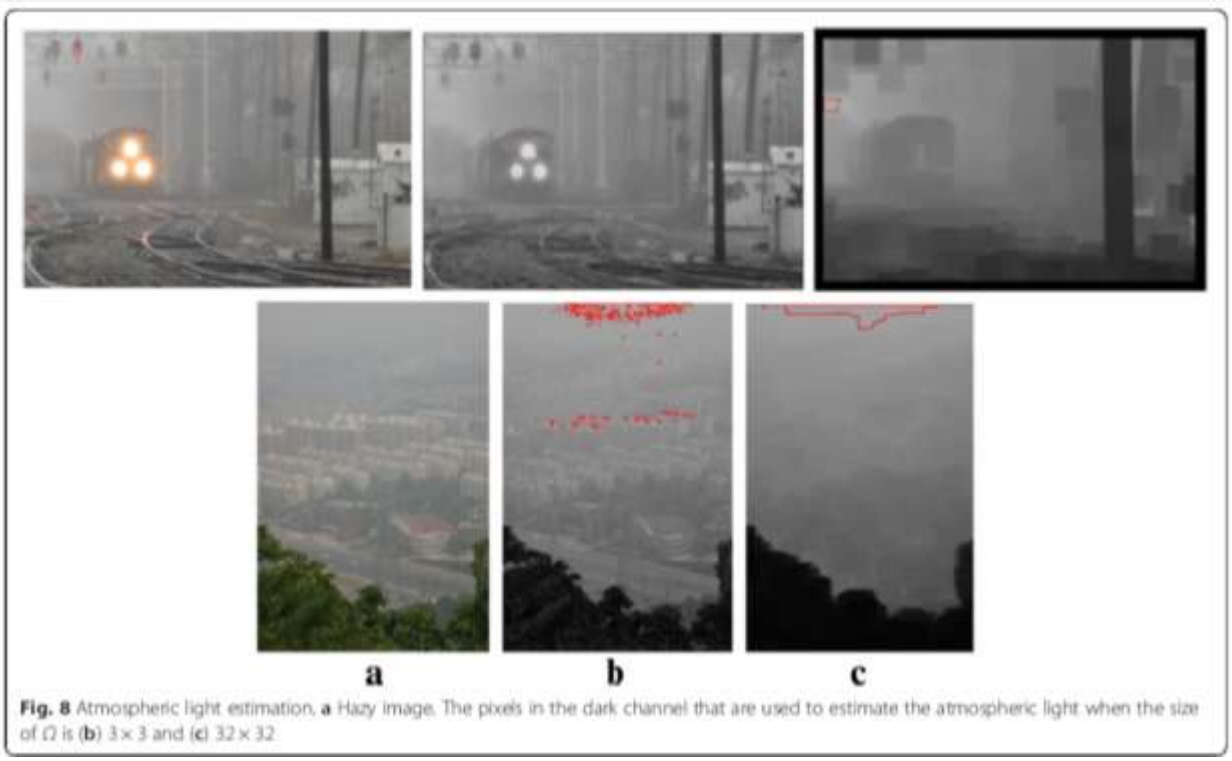

Fig. 8 Atmospheric light estimation. **a** Hazy image. The pixels in the dark channel that are used to estimate the atmospheric light when the size of Ω is (**b**) 3 × 3 and (**c**) 32 × 32

Figure 9 shows that the transmission map is indeed under-estimated when ~t is obtained as Eq. (9). The mean values of the ground-truth transmission maps, as shown in Fig. 9b, are 0.5616 and 0.6365, respectively. However, the mean values for the estimated transmission maps, as shown in Fig. 9c, are obtained as 0.5125 and 0.6086, respectively. When the transmission map is obtained as Eq. (17) by using ω = 0.9, the under-estimation of the transmission map is considerably decreased, as shown in Fig. 10a, c, where the mean values are obtained as 0.5225 and 0.6058, respectively. Xu et al.

explicitly addressed the aforementioned under-estimation problem of the

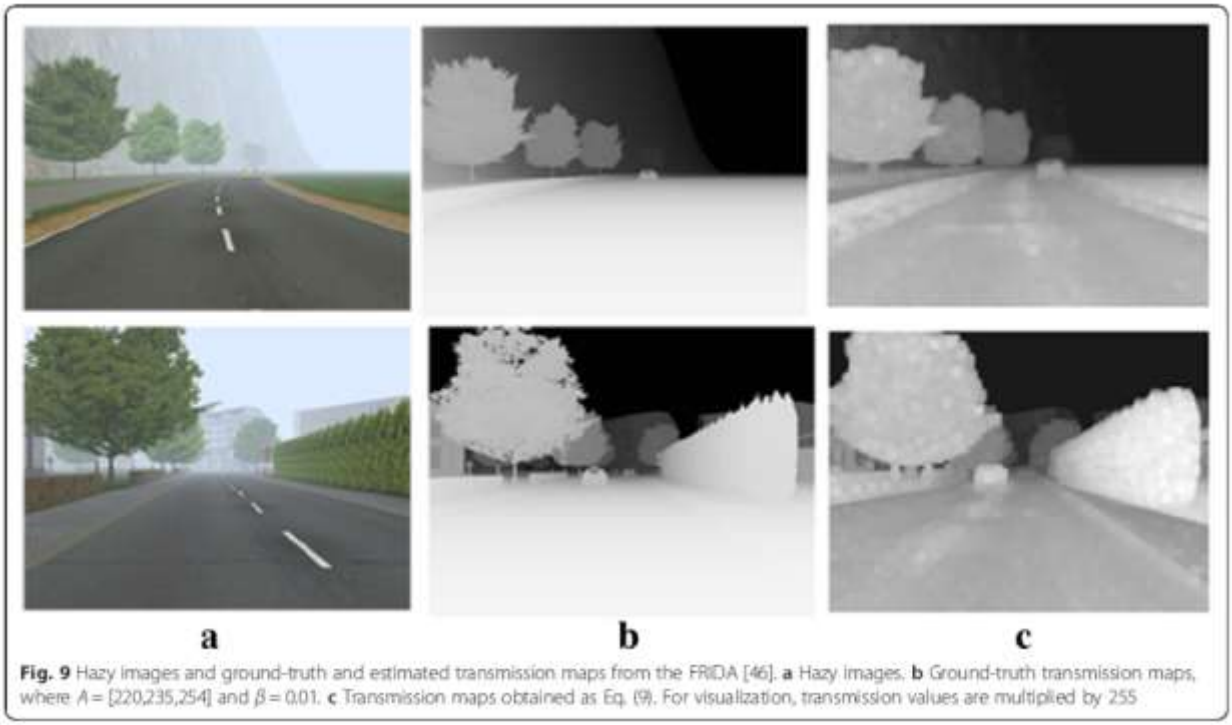

Fig. 9 Hazy images and ground-truth and estimated transmission maps from the FRIDA [46]. **a** Hazy images. **b** Ground-truth transmission maps, where $A = [220,235,254]$ and $\beta = 0.01$. **c** Transmission maps obtained as Eq. (9). For visualization, transmission values are multiplied by 255

transmission map and simply added a positive value $\rho \in [0.08, 0.25]$ to the transmission map:

$$\tilde{t}(x) = 1 - \min_{y \in \Omega(x)} \left(\min_{c} \frac{I^c(y)}{A^c} \right) + \rho. \tag{18}$$

Figure 10b, d shows the estimated transmission maps when $\rho = 0.08$ is added, where the mean values are obtained as 0.5494 and 0.6431, respectively. The addition of ρ also plays a similar role of t_0 in Eq. (11), making the minimum value of the transmission map be ρ. The under-estimation can be partly solved by using Eq. (17) or (18); however, the values of ω and ρ need to be carefully chosen. To this end, we measured the RMSE values between the ground-truth and estimated transmission maps for different ω and ρ values by using 66 synthetic test images from the FRIDA. Figure 11a, b indicates that ω around 0.9 and ρ around 0.12 are effective. An adaptive scheme also needs to be developed for a better compensation of the under-estimation.

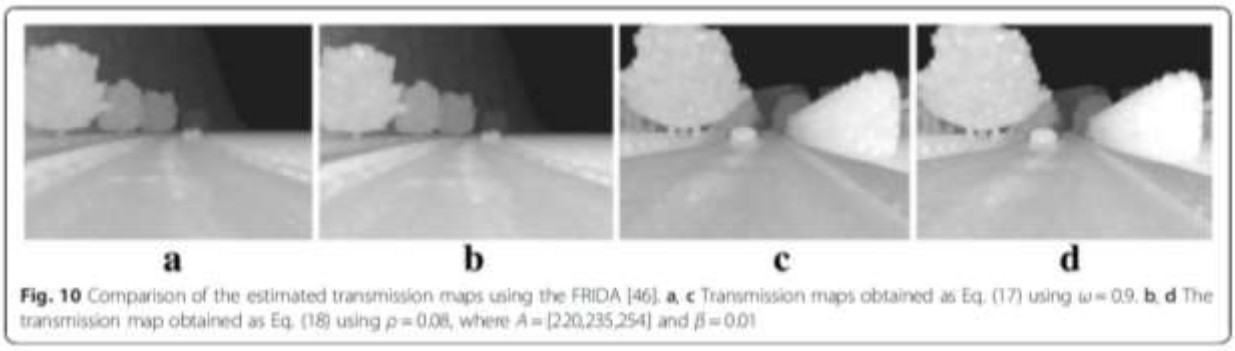

Fig. 10 Comparison of the estimated transmission maps using the FRIDA [46]. **a**, **c** Transmission maps obtained as Eq. (17) using $\omega = 0.9$. **b**, **d** The transmission map obtained as Eq. (18) using $\rho = 0.08$, where $A = [220,235,254]$ and $\beta = 0.01$

3.4. Transmission map refinement:

Incorrect estimation for the transmission map can lead to some problems such as false textures and blocking
artifacts. In particular, the block-min process of Eq. (4) decreases the apparent resolution of the dark channel,
resulting in blurry transmission maps. For this reason, many methods have been developed to further sharpen the transmission map [10, 11, 13, 14, 16–20, 22, 24]. In, it is especially mentioned that many dehazing methods differ in the way of smoothing the transmission map. Table 4 lists post-filtering methods used to improve the accuracy of the transmission map.

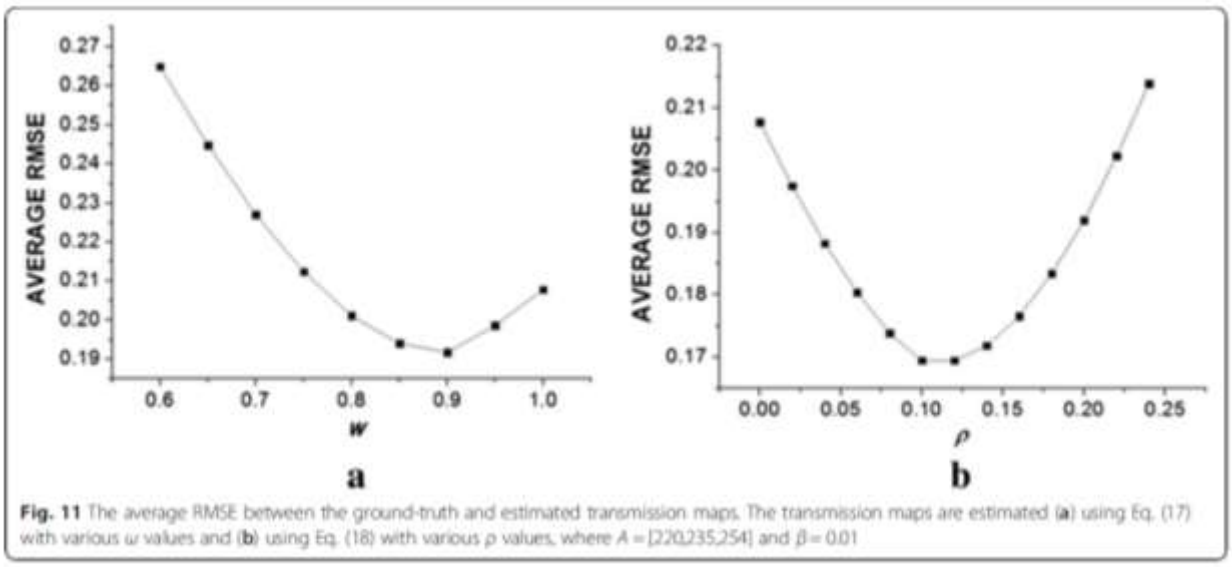

Fig. 11 The average RMSE between the ground-truth and estimated transmission maps. The transmission maps are estimated (**a**) using Eq. (17) with various ω values and (**b**) using Eq. (18) with various ρ values, where $A = [220,235,254]$ and $\beta = 0.01$

improve the accuracy of the transmission map. Some filtering methods, such as the Gaussian and Guided filters, use only transmission maps, whereas the other methods, such as soft matting, cross-bilateral filter, and guided filter, exploit a hazy color image as a guidance signal. Each method and its performance are analyzed in the following subsections.

3.4.1. Relativity of Gaussian (RoG):

In proposed system, we use guided filter and Relativity of Gaussian for enhancement of transmission map. Relativity of Gaussian can be applied to hazy images for detail enhancement. We adopt detail improvement based on Relativity of Gaussian (RoG) to boost the structure and details within the image while preserving the edges. RoG is applied to the reconstructed Y channel and a smoothened result is achieved. Relativity of Gaussian is utilized for the transmission map t(x) and $t_Y(x)$. Guided filter is applied to the transmission map where guidance image is the Relativity of Gaussian map is obtained. RoG based

detail enhancement is to improve the detail within the image while preserving the edges. Edge preserving smoothening can be split in to two: Local filter and Global optimization. Local filter will introduce Gibbs phenomenon resulting ringing and staircase distortions on edges. Global optimization focuses on comparatively small variance suppression. Local regularization is called RoG that is optimized to define the corners on a selective scale. In our work, $\sigma\sigma$ 1 and $\sigma 2$ are two parameters $\sigma 1$ is set as 10 and $\sigma 2$ is set as 20.

$$R = \left| \frac{G_{\sigma 1} * \nabla S}{G_{\sigma 2} * \nabla S} \right| \text{s.t. } \sigma_1 < \sigma_2 \quad (19)$$

3.4.1. Guided Filter:

The guided or directed filter has edge preservation and gradient preservation (19) capabilities. We made use of the linear local model for the estimation of the guided image. Guided filter is commonly used for dehazed application especially for preserving the details and structure present in the image. In the existing system, Laplacian filter is implemented for the enhancement of transmission map, output gradients are deducted from the initial transmission map mean filter is implemented for smoothening. In our work, we used a Guided filter for smoothening and detail enhancement of the image.

3.5. Reconstruction of Haze Free Image:

In final stage after computing all the parameters is to reconstruct the improved quality image with minimized haze influence. The image reconstruction process is given by:

$$\mathbf{J(x)} = \frac{I - A}{\max(t(x), t_0)} + A \quad (20)$$

$$J_y(\mathbf{x}) = \frac{I - A_y}{\max(t_y(x), t_0)} + A_y \quad (21)$$

where t_0 is a constant, **J(x)** and $\boldsymbol{JJyy}$**(x)** is the image reconstructed using the color space of RGB and is the image reconstruction using the color space of YCbCr.

$$\mathbf{R(x)} = \boldsymbol{\alpha J}\ (\boldsymbol{x}) + (\mathbf{1} - \boldsymbol{\alpha}) \boldsymbol{Jy}(\boldsymbol{x}) \quad (23)$$

To combine **J(x) and** $\boldsymbol{Jy}$**(x)** images, a parameter **α** is used as weight**.** R(x) is the final reconstructed image. The value of α is set to 0.5.

4. Result Analysis:

4.1. Qualitative Analysis:

Fig. 2. (a) Input Image (b) DCP for RGB color space (c) DCP for Y channel of YCbCr color space (d) Postion of airlight by I_{dark} and I_{dark_Y}

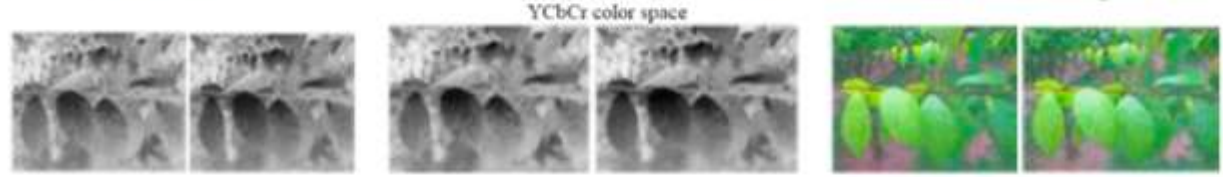

(e) Transmission map RGB and Y channel (f) Enhancement of transmission map with RoG (g) Image reconstructed from RGB and Image reconstructed from YCbCr

(h)Output image (i) Colores et.al[3] (j) Proposed Method

Fig 3. a) Input hazy image b) Colores et.al[3] c) Proposed Method d) ground truth

Fig. 4. a) Input Hazy Image b) Colores et.al[3] c) Proposed Method d) ground truth

Fig. 5. a) Input Hazy Image b) Colores et.al[3] c) Proposed Method d) ground truth

Colores et.al[3] result is haze free but it's color contrast is high and edges are not clear as in the reference image. Images obtained from the proposed method. From the qualitative assessment, it is clear that the result of the proposed method appears to be realistic, visually pleasing and almost similar to the ground truth image.

4.2. Quantitative Analysis:

The different evaluation measures employed to compute the performance of the proposed algorithm are SSIM, PSNR**,** BRISQUE and NIQE. We have performed the quantitative analysis in two ways. In the first case, test is conducted with the images where reference images or ground truth images are available and in the second case, where the reference images are not known or available. The metrics SSIM and PSNR are computed for the hazy images where reference image is available whereas BRISQUE and NIQE is computed for the images where ground truth images are not present. In both the above said cases, proposed technique outperforms the existing method.

4.2.1. SSIM and PSNR (evaluation measure used when ground truth images are present):

The SSIM(21) (Structural Similarity Index) is a technique for assessing the similarity or closeness of the result image with the ground truth image. This is a good evaluation metric for identifying the structures and the edges present in the resultant output image. The range of the SSIM is from 0 to 1. PSNR (Peak Signal to Noise Ratio) denotes the quality of the reconstructed image by comparing with the ground truth of the image. PSNR is computed using the given equation and it is represented in decimals.

$$\mathbf{PSNR = 10\ log_{10}(\frac{MAX^2}{MSE})} \tag{24}$$

where MAX denote max intensity of input image and MSE is error.

Table 2. Quantitative Analysis Performance Evaluation

Image	Existing Method[4]		**Proposed Method**	
	SSIM	PSNR (dB)	**SSIM**	**PSNR (dB)**
Leaf	0.5719	35.9990	**0.9149**	**40.9439**
Building	0.5094	38.5463	**0.8550**	**42.0662**
City	0.5429	36.7623	**0.8126**	**43.0335**
River	0.6114	20.6935	**0.8976**	**40.0294**
Trees	0.7561	39.2957	**0.9157**	**42.7431**

4.2.2. BRISQUE and NIQE (evaluation measure used when ground truth images are not present or available):

BRISQUE (Blind Reference less Image Spatial Quality Evaluator) (23) is an evaluation measure usually used in image enhancement where the ground truth

image is not known to the researchers. This metric is a quality for is computed based on the spatial feature. A lower score shows a better quality of perception. BRISQUE is a spatial domain-based metric which computes the naturalness of an image based on the Image Quality Assessment (IQA). It is inspired from the concept of considering the adjacent luminance values and estimating the statistical products of those values. In this model, parameters are further quantified to estimate the naturalness of the image. NIQE (Naturalness Image Quality Evaluator) (24) is an evaluation measure computed based on the naturalness of an image. This metric is a no-reference image quality score. A lower score shows a better quality of perception. NIQE metric is inspired from the concept of computing statistical characteristics that depends on the Natural Scene Statistic (NSS). NIQE apply NSS features from patches of the image and fitting Multivariate Gaussian Model (MVG). The quality of the distorted image is expressed as:

$$\mathbf{D}(\upsilon_1, \upsilon_2, \sum_1, \sum_2) = \sqrt{(\upsilon_1 - \upsilon_2)^T \left(\frac{\sum_1 + \sum_2}{2}\right)^{-1} (\upsilon_1 - \upsilon_2)} \qquad (25)$$

where $\Sigma 1$, $\Sigma 2$ and $\upsilon 1$, $\upsilon 2$ denote the covariance and average of the natural MVG model between the original and distorted images. Without ground truth images, we have calculated performance evaluation using NIQE and BRISQUE. Table 2 describe quality analysis of existing method and proposed method using SSIM and PSNR. The highest value of SSIM and PSNR indicates better result. Table 3 assesses the naturalness of test images using BRISQUE and NIQE. The smaller BRISQUE and NIQE values, better the result.

Table 3. Quantitative Analysis Performance Evaluation

Image	Existing Method[4]		**Proposed Method**	
	BRISQUE	NIQE	**BRISQUE**	**NIQE**
Road	44.4183	28.6463	**42.6199**	**23.1209**
House	48.6075	20.9788	**44.6079**	**15.6829**
Cons	44.7045	28..1794	**43.5352**	**20.5544**
Forest	44.7045	22.9675	**43.4604**	**16.3344**

5. Conclusion:

Usually, the natural weather conditions such as haze or fog hinder the visibility and aesthetic view of a scene. An improved image dehazing system has been proposed exploring the concept of improved Dark Channel Prior (DCP) and Relativity of Gaussian (RoG) with guided filter. Results show that the existing method produces over contrast, over enhancement and detailed information is hidden and is not properly identified. So, this improved method calculates the transmission map and applied Relativity of Gaussian and Guided filter to enhance the transmission map. This work provides good performance for the task of obtaining haze-less image both qualitative and quantitative manner. Experimental results show that the proposed method estimates haze more accurately, the reconstruct the images are more realistic and detailed information is restored.